Mesothelin/CD3 Half-Life–Extended Bispecific T-Cell Engager Molecule Shows Specific Tumor Uptake and Distributes to Mesothelin and CD3-Expressing Tissues

Frans V. Suurs[1], Grit Lorenczewski[2], Julie M. Bailis[3], Sabine Stienen[2], Matthias Friedrich[2], Fei Lee[3], Bert van der Vegt[4], Elisabeth G.E. de Vries[1], Derk Jan A. de Groot[1], and Marjolijn N. Lub-de Hooge[5,6]

[1]Department of Medical Oncology, University Medical Center Groningen, Groningen, The Netherlands; [2]Amgen Research Munich GmbH, Munich, Germany; [3]Amgen Inc., South San Francisco, California; [4]Department of Pathology, University Medical Center Groningen, Groningen, The Netherlands; [5]Department of Clinical Pharmacy and Pharmacology, University Medical Center Groningen, Groningen, The Netherlands; and [6]Department of Nuclear Medicine and Molecular Imaging, University Medical Center Groningen, Groningen, The Netherlands

Bispecific T-cell engager (BiTE) molecules exert antitumor activity by binding one arm to CD3 on cytotoxic T cells and the other arm to a tumor-associated antigen. **Methods:** We generated a fully mouse cross-reactive mesothelin-targeted BiTE molecule that is genetically fused to an Fc-domain for half-life extension, and we evaluated the biodistribution and tumor targeting of a ^{89}Zr-labeled mesothelin half-life–extended (HLE) molecule in 4T1 breast cancer–bearing syngeneic mice with PET. The biodistribution of 50 μg of ^{89}Zr-mesothelin HLE BiTE was studied over time by PET imaging in BALB/c mice and revealed uptake in tumor and lymphoid tissues with an elimination half-life of 63.4 h. **Results:** Compared with a nontargeting ^{89}Zr-control HLE BiTE, the ^{89}Zr-mesothelin HLE BiTE showed a 2-fold higher tumor uptake and higher uptake in lymphoid tissues. Uptake in the tumor colocalized with mesothelin expression, whereas uptake in the spleen colocalized with CD3 expression. Evaluation of the effect of protein doses on the biodistribution and tumor targeting of ^{89}Zr-mesothelin HLE BiTE revealed for all dose groups that uptake in the spleen was faster than in the tumor (day 1 vs. day 5). The lowest dose, 10 μg, of ^{89}Zr-mesothelin HLE BiTE had higher spleen uptake and faster blood clearance than the higher doses, 50 and 200 μg. ^{89}Zr-mesothelin HLE BiTE tumor uptake was similar at all doses. **Conclusion:** The mesothelin HLE BiTE showed specific tumor uptake, and both arms contributed to the biodistribution profile. These findings support the potential for clinical translation of HLE BiTE molecules.

Key Words: half-life–extended bispecific T-cell engager (HLE BiTE) molecule; PET imaging; bispecific antibody; syngeneic mouse model; cancer-immunotherapy

Bispecific constructs engaging T cells are a novel form of cancer immunotherapy (1). They engage T cells to tumors, leading to T-cell–mediated tumor-cell killing irrespective of T-cell clonality. The number of T-cell–engaging bispecific constructs has been increasing over the last few years, with 38 constructs in clinical oncology trials in 2019 (2,3).

Bispecific T-cell engager (BiTE; Micromet AG) molecules are T-cell–engaging bispecific constructs of approximately 53 kDa that exist as 2 single-chain variable fragments (scFv) connected by a short linker (4). One scFv binds T cells via the CD3 receptor, and the other scFv binds the tumor cell via a tumor-associated antigen. Blinatumomab, a BiTE molecule targeting CD19 and CD3, has been approved by the Food and Drug Administration and European Medicines Agency for the treatment of B-cell acute lymphoblastic leukemia. Other BiTE molecules are in clinical evaluation (2,5–7). BiTE molecules show rapid clearance with a serum half-life of a few hours (8,9) To maintain therapeutic serum concentrations, they are administered via continuous intravenous infusion.

To prolong plasma half-life and allow less frequent dosing, BiTE molecules have been genetically fused to an Fc domain. This results in a half-life–extended (HLE) BiTE molecule with a molecular weight of approximately 106 kDa (Supplemental Fig. 1A; supplemental materials are available at http://jnm.snmjournals.org) (10,11). In nonhuman primates, HLE BiTE molecules showed an extended serum half-life compatible with intermittent dosing (11).

Studies in immunocompetent mice showed the complexity of the biodistribution of T-cell–engaging bispecific constructs. Increasing the affinity for CD3 of a CLL-1 T-cell–engaging bispecific antibody reduced its plasma half-life (12). A high-affinity CD3-targeting murine EpCAM BiTE molecule showed high lymphoid uptake and low tumor uptake (13). Moreover, uptake of HER2 T-cell–engaging bispecific antibodies was higher in lymphoid tissues and lower in the tumor when CD3 affinity increased (14). Biodistribution of the CEA-targeted BiTE molecule ^{89}Zr-AMG 211 was evaluated in patients with gastrointestinal adenocarcinomas. PET showed uptake in tumor lesions, although at moderate levels, as well as in lymphoid organs (9).

Currently, 8 HLE BiTE molecules are in clinical trials, of which 4 are in solid tumors (NCT03319940, NCT03792841, NCT04117958, and NCT04260191) (15). Increasing the half-life and molecular weight of a protein might influence the biodistribution and improve tumor targeting (16,17). There are few data regarding the biodistribution and tumor targeting of HLE BiTE molecules. Therefore, we aimed to explore this preclinically with whole-body molecular imaging using PET and ex vivo analyses.

We used an HLE BiTE molecule targeting murine CD3 and murine mesothelin (mesothelin HLE BiTE) that we radiolabeled with the PET isotope ^{89}Zr. ^{89}Zr is an attractive PET isotope because of its long half-life (78.4 h) and efficient labeling to proteins (18).

Mesothelin is an attractive therapeutic target because of its high expression on the cell surface of several human cancers, including mesothelioma, ovarian cancer, pancreatic adenocarcinoma, and triple-negative breast cancer (19). Mesothelin expression on normal cells is primarily in the mesothelial cell layer (19). Mesothelin HLE BiTE molecules have been reported, and multiple mesothelin-targeted drugs are currently in development (19–23).

Here, we report the biodistribution of the ^{89}Zr-labeled murine mesothelin HLE BiTE molecule in tumor-bearing syngeneic mice compared with a nontargeting control HLE BiTE molecule.

MATERIALS AND METHODS

HLE BiTE Molecules and Cell Lines

A mouse cross-reactive mesothelin scFv was generated using the commercially available mouse antimesothelin antibody MN-1 (200-301-A88; Rockland), and affinity matured to increase mesothelin binding. The murine mesothelin scFv was attached by a short linker to mouse CD3 and a mouse cross-reactive Fcγ-silenced Fc-domain (24), resulting in the mouse mesothelin HLE BiTE molecule. For a nontargeting HLE BiTE molecule, a BiTE molecule targeting human EpCAM and human CD3 was fused to a Fcγ-silenced human Fc. Amgen provided the murine mesothelin HLE BiTE molecule and the control HLE BiTE molecule.

The conjugation to tetrafluorophenol-N-succinyl-desferrioxamine-Fe (TFP-N-suc-DFO-Fe; ABX) and labeling with ^{89}Zr of the HLE BiTE molecules are described in the supplemental materials (13,25). Labeling of the HLE BiTE molecules with ^{89}Zr resulted in [^{89}Zr]Zr-DFO-N-suc-HLE BiTE molecules (^{89}Zr-HLE BiTE molecules).

The mesothelin-positive murine mammary carcinoma cell line 4T1 (ATCC) was cultured in RPMI-1640 medium (Invitrogen) containing 10% fetal calf serum (Bodinco BV). Cells were used between passages 5 and 20 after thawing and cultured under aseptic conditions at 37°C in an incubator providing a humidified atmosphere of 5% CO_2. The cells were routinely tested for the presence of *Mycoplasma*.

Animal Experiments

All animal experiments were approved by the Institutional Animal Care and Use Committee of the University of Groningen. Eight- to 10-wk-old female BALB/c mice (BALB/cOlaHsd; Envigo) were injected with 5×10^4 4T1 cells in 50 μL of RPMI-1640 in the lower mammary fat pad after 1 wk of acclimatizing. Mice were allocated randomly to the groups.

Tracers (4–5 MBq) were retroorbitally injected when tumors reached approximately 200 mm^3. Retroorbital injections were chosen similarity in distribution to intravenous tail-vein injection, with no increased discomfort, and facile execution (26,27). The mice were anesthetized with isoflurane/medical air inhalation (5% induction, 2.5% maintenance) during all procedures. Whole-body radioactivity in the mice was measured with a calibrated dose-calibrator (Comecer).

Small-animal PET scans were acquired with a Focus 220 rodent scanner (CTI Siemens). The data were reconstructed as previously described (28).

Scans were analyzed with PMOD software (version 4.004; PMOD Technologies). Volumes of interest were drawn as spheres based on the weight of organs found in the biodistribution. Data are expressed as SUV$_{mean}$.

PET scans were visualized as maximum-intensity projections scaled to the same maximum, allowing comparison between groups. Blood elimination half-life was calculated using 1-phase decay (Prism 7; GraphPad).

The in vivo biodistribution of 50 μg of ^{89}Zr-mesothelin HLE BiTE was visualized in 8 tumor-bearing BALB/c mice by small-animal PET scans at 1, 3, 5, 7, and 9 d after injection. This dose was based on previous experience with immune cell–targeting tracers (29).

The effect of the protein dose on the biodistribution and specific uptake of ^{89}Zr-mesothelin HLE BiTE was investigated by comparing 10, 50, and 200 μg of ^{89}Zr-mesothelin HLE BiTE and 50 μg of ^{89}Zr-control HLE BiTE at 1, 3, and 5 d after injection. After the last imaging time point, an ex vivo biodistribution study was performed. All dose groups had 6 tumor-bearing BALB/c mice. Organs of interest and tumor were collected, weighed, and measured in a calibrated Wizard γ-counter (PerkinElmer). Axillary lymph nodes were discarded from further analysis since their low weight resulted in highly variable values. Counts of known standards were used to convert counts into injected dose. Tissue radioactivity is expressed as percentage injected dose per gram. Relevant tissues were fixed in formalin and embedded in paraffin for further analysis.

Ex Vivo Tissue Analysis

Formalin-fixed paraffin-embedded blocks of tumor and spleen were sliced into 4-μm sections. Tissue slides were exposed overnight to phosphor screens (PerkinElmer) in x-ray cassettes. The imaging screens were read out by the Cyclone storage Phosphor System (PerkinElmer), and autoradiography images were analyzed with ImageJ, version 1.52p. These slides were stained with hematoxylin and eosin (H&E) to assess tissue morphology. To quantify autoradiography data, regions of interest were identified in H&E-stained slides. These regions were imported onto the autoradiography images and quantified. Values were normalized for activity injected.

In subsequent sections of the H&E-stained slides, the presence of murine mesothelin and murine CD3 was visualized with immuno-histochemical staining. For murine CD3, after antigen retrieval for
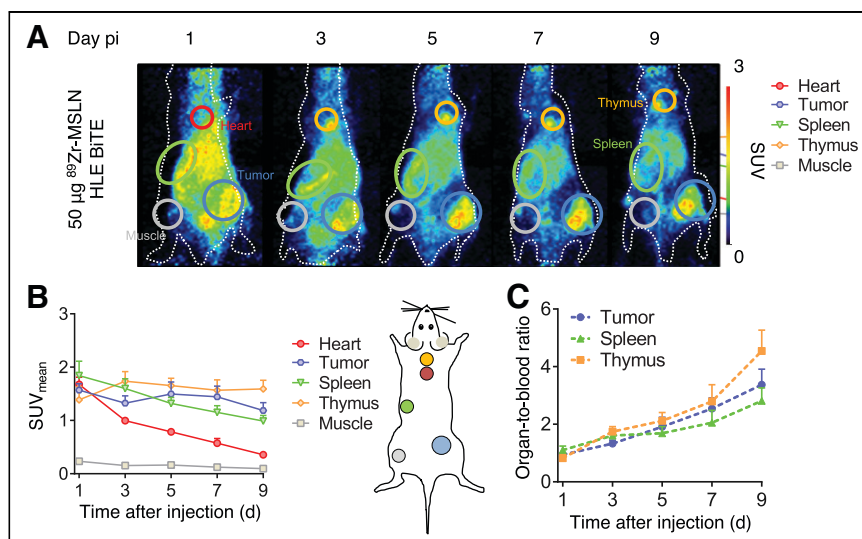

FIGURE 1. PET scans over time after administration of 50 μg of ^{89}Zr-mesothelin HLE BiTE in 4T1-tumor–bearing mice ($n = 8$). (A) Representative maximum-intensity projections of PET images up to 9 d after tracer injection. Encircled are spleen (green), heart (red), tumor (blue), and thymus (yellow). (B) Image quantification of heart, tumor, spleen, thymus, and muscle expressed as SUV$_{mean}$. (C) Image quantification expressed as organ-to-blood ratios. Data are presented as mean ± SD. MSLN = mesothelin; pi = after injection.

15 min at 95°C with a citrate buffer at pH 6, a rabbit antimouse anti-CD3 antibody, clone SP7 (ab16669; Abcam), was used in a 1:50 dilution. For mesothelin, antigens were retrieved in a Tris/HCl buffer at pH 9 for 15 min of incubation at 95°C, followed by overnight incubation with a rabbit antirabbit antimesothelin antibody (R32262; NSJ Bioreagents) in a 1:50 dilution. Thereafter, a peroxidase-conjugated goat antirabbit antibody (Dako) and 3–3'-diaminobenzidine (DAB) were added to visualize peroxidase activity. Necrotic areas on H&E-stained liver sections were quantified in QuPath (30). With a limulus amebocyte lysate assay (Endosafe-PTS; Charles River), bacterial endotoxins were quantified in the parental and conjugated mesothelin HLE BiTE and in the final tracer solution.

The gastrointestinal tract was exposed overnight to a phosphor plate at −20°C 9 d after injection of 50 μg of ^{89}Zr-mesothelin HLE BiTE. Thereafter, sections of the tissue were embedded with TissueTek optimal-cutting-temperature compound (Sakura) and stained with H&E.

Statistical Methods

SUV$_{mean}$ PET scan data are expressed as mean ± SD. An ANOVA among uptake of multiple groups was followed by a post hoc Tukey multiple-comparison test. P values of 0.05 or less were considered significant.

Ex vivo biodistribution data are presented as median percentage injected dose per gram, with interquartile range. On these data, an ANOVA among uptake of multiple groups was performed with the Kruskal–Wallis test. When statistically significant differences were found, a post hoc Bonferroni-corrected Mann–Whitney U test was performed. Between a pair of groups, the similarity was tested with a Mann–Whitney U test.

All statistical tests were performed in Prism (version 7; GraphPad).

RESULTS

Conjugation and Radiolabeling of HLE BiTE Molecules

The binding affinity of the parental mesothelin HLE BiTE was 3.0 nM for mouse mesothelin expressed on 4T1 cells and 26.8 nM for CD3 expressed on T cells for mouse CD3 (Supplemental Figs. 1B and 1C). The 4T1 cell line expresses 5933 mesothelin molecules per cell (Supplemental Fig. 1D). This mesothelin expression is relatively low compared with the ovarium carcinoma cell line OVCAR8 and other human mesothelin-positive cancer cell lines (Supplemental Fig. 1E) (20).

The parental mesothelin HLE BiTE molecule engaged mouse T cells to kill 4T1 tumor cells, with half-maximal lysis

of 29.15 pM (Supplemental Fig. 1F). Mesothelin HLE BiTE activity was specific for mesothelin-expressing cells, as no activity was observed against the mesothelin-negative cell line B16F10 (Supplemental Fig. 1G). The nontargeting control HLE BiTE molecule did not have activity against either 4T1 or B16F10 cells, as expected.

Conjugation on the HLE BiTE molecules resulted in HLE BiTE:DFO end ratios of 1:2.6 and 1:2.3, respectively. Conjugation of the mesothelin HLE BiTE did not affect its ability to engage T cells
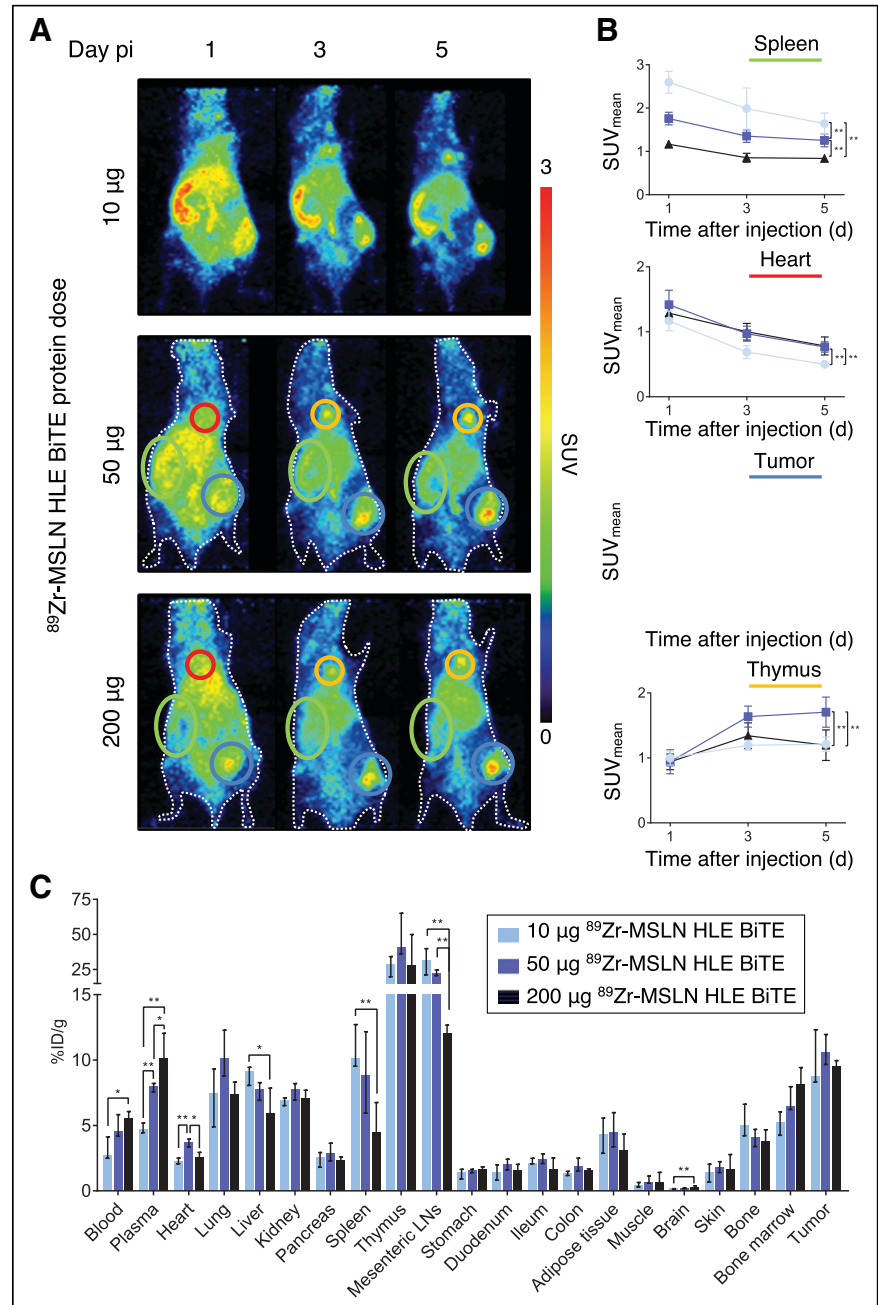

FIGURE 2. Dose-dependent biodistribution of ^{89}Zr-mesothelin HLE BiTE in 4T1-tumor–bearing mice. (A) Representative maximum-intensity projections of PET images at 1, 3, and 5 d after injection of 10, 50, or 200 μg ^{89}Zr-mesothelin HLE BiTE ($n = 6$ for 10- and 50-μg doses, $n = 5$ for 200-μg dose). Encircled are spleen (green), heart (red), tumor (blue), and thymus (yellow). (B) PET quantification of spleen, heart, tumor, and thymus; data are presented as mean ± SD. (C) Ex vivo biodistribution with data presented as median with interquartile range. LNs = lymph nodes; MSLN = mesothelin; pi = after injection. *$P \leq 0.05$. **$P \leq 0.01$
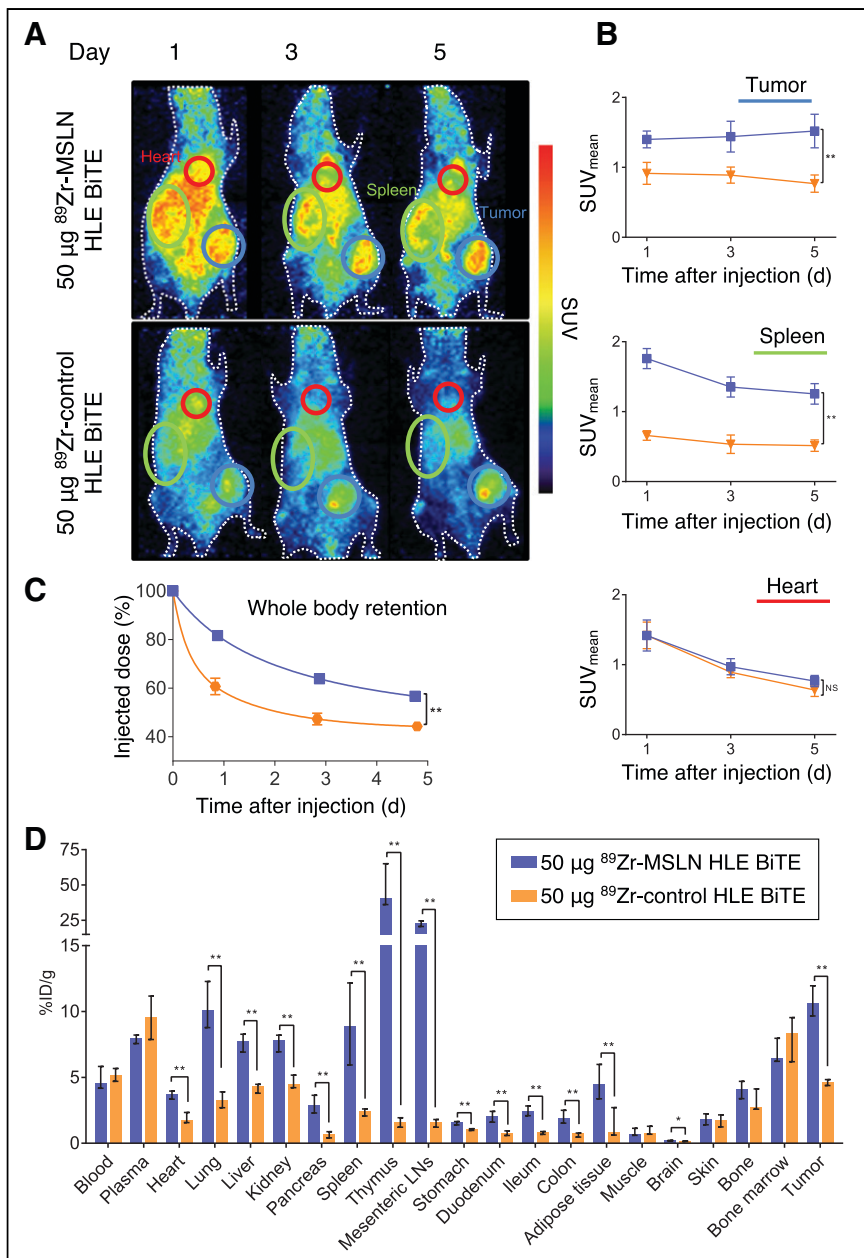
FIGURE 3. Biodistribution of 50 μg of ^{89}Zr-mesothelin HLE BiTE compared with 50 μg of ^{89}Zr-control HLE BiTE. (A) Representative maximum-intensity projections of PET images at 1, 3, and 5 d after injection of ^{89}Zr-mesothelin HLE BiTE ($n = 6$) or ^{89}Zr-control HLE BiTE ($n = 6$). Encircled are spleen (green), heart (red), and tumor (blue). (B) PET quantification of tumor, spleen, and heart. (C) Whole-body retention measured by dose calibrator. Data are presented as mean ± SD. (D) Ex vivo biodistribution with data presented as median with interquartile range. LNs = lymph nodes; MSLN = mesothelin. *$P \le 0.05$. **$P \le 0.01$

and target cells, shown by maintained in vitro cytotoxicity and T-cell activation (Supplemental Figs. 2A–2C). Also, the conjugated mesothelin HLE BiTE was intact, with a single protein peak at 280 nm on the chromatogram (Supplemental Fig. 2D).

PET Imaging of ^{89}Zr-Mesothelin HLE BiTE over Time

PET scanning after 50 μg of ^{89}Zr-mesothelin HLE BiTE administration was performed at 1, 3, 5, 7, and 9 d and revealed uptake in the tumor, spleen, thymus, and liver (Fig. 1A). Time to reach the maximum uptake varied for organs and tumor (Fig. 1B). Spleen uptake was already highest at day 1 (SUV$_{mean}$,

1.84 ± 0.25) and decreased, whereas thymus uptake was maximal at day 3 (SUV$_{mean}$, 1.74 ± 0.17) and remained stable thereafter. Maximum tumor uptake was reached at day 5 (SUV$_{mean}$, 1.50 ± 0.21).

Organ-to-blood ratios increased between days 1 and 9 to 4.5 ± 0.7 for the thymus, 3.4 ± 0.5 for the tumor, and 2.8 ± 0.4 for the spleen, since blood levels decreased (Fig. 1C). ^{89}Zr-mesothelin HLE BiTE blood elimination half-life, based on the heart blood pool, was 63.4 h ($R = 0.96$). Day 5 was chosen to compare ex vivo biodistribution, when organ-to-blood ratios were 2.1 ± 0.3 for the thymus, 1.9 ± 0.3 for the tumor, and 1.7 ± 0.2 for the spleen.

Dose-Dependent Biodistribution of ^{89}Zr-Mesothelin HLE BiTE

On day 1 after 10 μg of ^{89}Zr-mesothelin HLE BiTE administration, a high spleen-to-blood ratio (2.26 ± 0.33) visualized the spleen on PET scans, in contrast to the 50- and 200-μg groups (1.26 ± 0.15 and 0.92 ± 0.13, respectively; Fig. 2A; Supplemental Fig. 3A). Spleen SUV$_{mean}$ inversely correlated with protein dose, indicating target saturation (Fig. 2B). Blood SUV$_{mean}$ for the 10-μg dose was lower than for the higher doses. As a consequence, on day 5 tumor uptake for the 10-μg dose was lower than that for the 50-μg dose, but no difference between the tumor-to-blood ratios was found (Supplemental Fig. 3A). In the thymus, no relation between uptake and protein dose was seen (Fig. 2B). However, uptake was higher for the 50-μg dose than for 10 μg or 200 μg.

Ex vivo analysis on day 5 confirmed the PET findings and revealed dose-dependent uptake in the mesenteric lymph nodes (Fig. 2C; Supplemental Table 1).

Biodistribution of ^{89}Zr-Mesothelin HLE BiTE Compared with a Nontargeting ^{89}Zr-Control HLE BiTE Molecule

Tumor SUV$_{mean}$ after 50 μg of ^{89}Zr-mesothelin HLE BiTE increased from day 1 (1.40 ± 0.11) to day 5 (1.52 ± 0.22), whereas for 50 μg of ^{89}Zr-control HLE BiTE, tumor uptake decreased from day 1 (0.91 ± 0.14) to day 5 (0.77 ± 0.11) (Figs. 3A and 3B). ^{89}Zr-control HLE BiTE did not show uptake in the spleen or thymus. Although blood levels obtained with both tracers were similar, whole-body radioactivity levels showed that the whole-body clearance of ^{89}Zr-control HLE BiTE was faster than that of ^{89}Zr-mesothelin HLE BiTE (Fig. 3C).

Ex vivo biodistribution at day 5 confirmed the similar blood levels and specific uptake of ^{89}Zr-mesothelin HLE BiTE in the tumor, spleen, and thymus compared with the control HLE BiTE
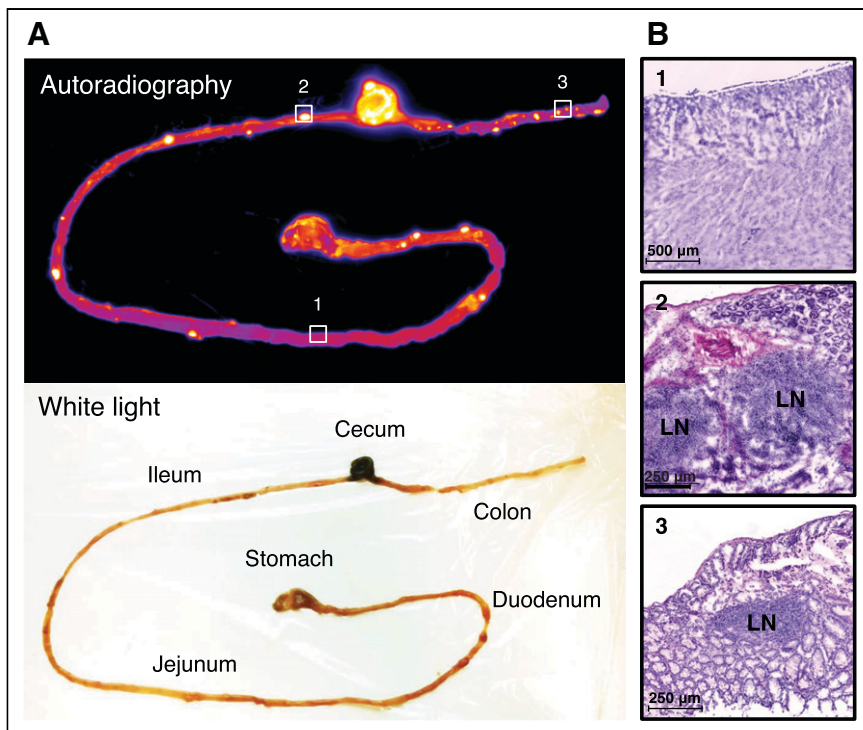
FIGURE 4. (A) Activity retention in gastrointestinal tract 9 d after injection of 50 µg of ^{89}Zr-mesothelin HLE BiTE in 4T1-tumor–bearing BALB/c mouse. (B) H&E staining of frozen sections of highlighted areas. LN = lymph node.

(Fig. 3D; Supplemental Table 2). ^{89}Zr-mesothelin HLE BiTE uptake was also higher than the control level in the liver, kidney, lung, adipose tissue, and gastrointestinal tract.

White spots on the liver were observed ex vivo in the various ^{89}Zr-mesothelin HLE BiTE groups. H&E staining revealed areas of necrosis, whereas in the ^{89}Zr-control HLE BiTE group the liver tissue was unaffected. Higher protein doses of ^{89}Zr-mesothelin HLE BiTE showed an increased area affected by necrosis. Endotoxin measurements of mesothelin HLE BiTE and the conjugated stock, as well as the tracer solution, revealed no contaminations (Supplemental Fig. 4).

Ex Vivo Analysis of ^{89}Zr-Mesothelin HLE BiTE Uptake by Autoradiography and Immunohistochemistry

Autoradiography showed hot spots in the gastrointestinal tract of mice 9 d after receiving 50 µg of ^{89}Zr-mesothelin HLE BiTE (Fig. 4A). H&E staining of frozen sections identified the radioactivity localized in the gut-associated lymphoid nodes, consistent with binding of the tracer to T cells (Fig. 4B). Examining the slides 9 d after injection instead of 5 d might have increased the signal-to-background ratio (Fig. 1). Radioactivity hot spots in the spleen, identified 5 d after tracer injection, colocalized with the white pulp (Fig. 5A). Immunohistochemistry staining confirmed high CD3 expression in the white pulp, whereas mesothelin staining was negative. In contrast, for ^{89}Zr-control HLE BiTE, no hot spots and only a low homogeneous distribution were seen in the spleen. Quantification of autoradiography data confirmed the higher spleen uptake of ^{89}Zr-mesothelin HLE BiTE ($1{,}747 \pm 109.8$) than of ^{89}Zr-control HLE BiTE ($1{,}009 \pm 59.6$, $P < 0.01$). It also showed the high ^{89}Zr-mesothelin HLE BiTE signal in the CD3-rich white pulp ($2{,}763 \pm 119.2$) versus the red pulp ($1{,}516 \pm 86.9$) (Supplemental

Fig. 5). ^{89}Zr-mesothelin HLE BiTE autoradiography of the tumor showed that the radioactivity overlapped with mesothelin-expressing tumor tissue outside the necrotic core (Fig. 5B). The signal was not increased in tumor areas that contained CD3-positive cells. ^{89}Zr-control HLE BiTE uptake in tumor tissue was low, but higher local uptake matched with the small necrotic core (Fig. 5B; Supplemental Fig. 6). ^{89}Zr-mesothelin HLE BiTE autoradiography of tumor tissue with an adjacent lymph node showed radioactivity overlapping with CD3 expression in the lymph node and with mesothelin expression in the tumor. Interestingly, radioactivity in the adjacent lymph node was 2-fold higher than uptake in the tumor (Supplemental Fig. 7).

DISCUSSION

To our knowledge, this was the first biodistribution study with an HLE BiTE molecule. The mesothelin HLE BiTE showed specific uptake in the tumor and lymphoid organs. Uptake of the tracer in the spleen and mesenteric lymph nodes was dose-dependent. Mesothelin HLE BITE localized to the gut in the adjacent lymph nodes. Both targeting arms clearly contributed to the mesothelin HLE BiTE biodistribution, with spleen uptake correlating with the CD3 expression whereas tumor uptake related to mesothelin expression.

Two variables changed with the mesothelin HLE BiTE compared with the previously evaluated first-generation BiTE molecules. The half-life was extended by fusing the BiTE molecule to an Fc domain, and the affinity for the tumor-associated antigen (mesothelin, dissociation constant [K_d] = 3.0 nM) was higher than for CD3 (K_d = 26.8 nM). Our study showed that these modifications induced important differences in the biodistribution. The biodistribution of the first-generation BiTE molecule muS110, targeting mouse EpCAM (K_d = 21 nM), and mouse CD3 (K_d = 2.9 nM) was driven by its CD3 arm (13). For the mesothelin HLE BiTE molecule, both arms contributed to its biodistribution. Intratumoral uptake colocalized with mesothelin expression, and the maximum tumor uptake for mesothelin HLE BiTE was 6-fold higher than for muS110. Moreover, this maximum uptake was reached later, namely on day 5 versus at 6 h after administration. Other first-generation BiTE molecules also had lower tumor uptake in biodistribution studies in nude mice bearing human tumors. Depending on the BiTE molecule and tumor model used, uptake varied between 4% and 8% of the injected dose per gram at 24 h after administration (28,31).

Spleen uptake colocalized with CD3 presence in the white pulp. The Fcγ-silenced Fc domain of mesothelin HLE BiTE, and uptake in T-cell–rich white pulp versus lower uptake in the macrophage-rich red pulp, rendered Fc-mediated spleen uptake, if present, minimal. We found that 5,933 mesothelin molecules are expressed per 4T1 cell, whereas around 10^5 CD3 molecules are generally expressed per human T cell (32,33). In the spleen, this high CD3 expression possibly acts as a first "sink." This organ, which
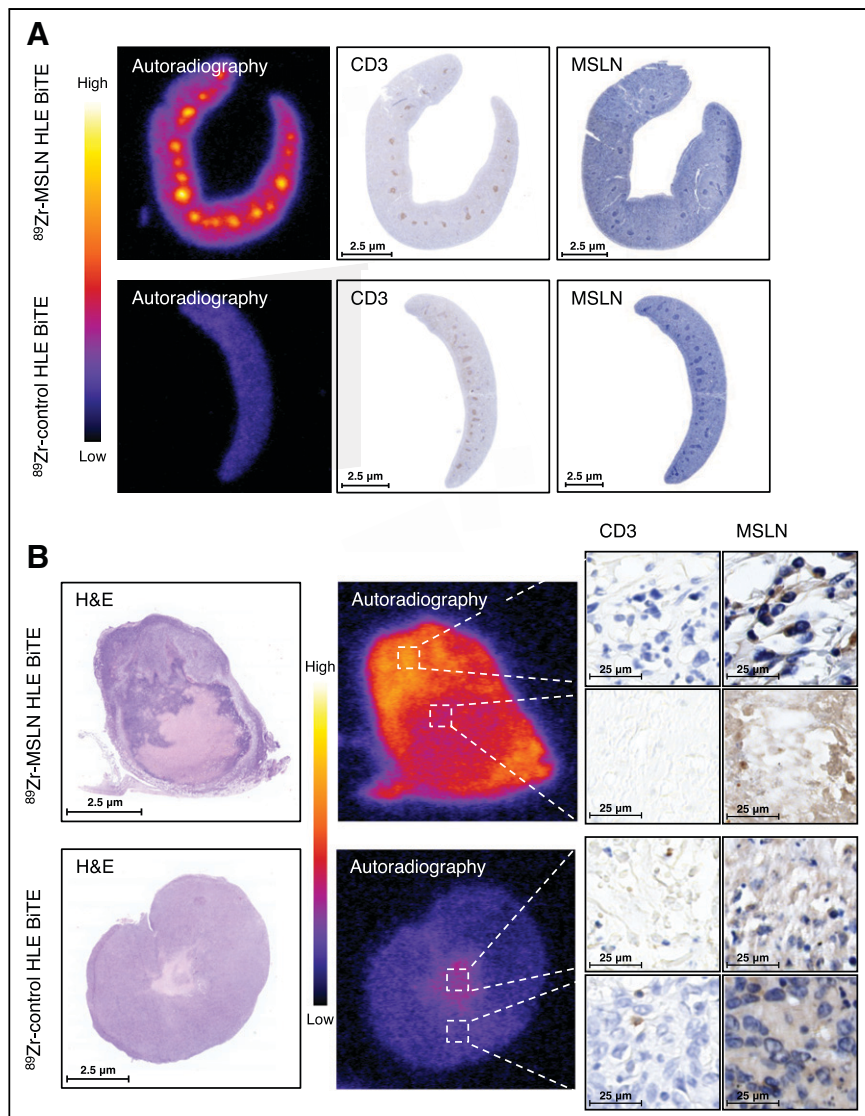
FIGURE 5. Ex vivo analysis of spleen and tumor tissue (4T1) 5 d after injection of 50 μg of ^{89}Zr-mesothelin HLE BiTE or 50 μg of ^{89}Zr-control HLE BiTE. (A) Spleen tissue. From left to right are shown tissue autoradiography, CD3 immunohistochemistry, and mesothelin immunohistochemistry. (B) Tumor tissue. From left to right are shown H&E and tissue autoradiography, followed by CD3 immunohistochemistry and mesothelin immunohistochemistry of high- and low-uptake areas. In H&E panel, necrotic core is shown as lighter-staining region. MSLN = mesothelin.

affinity of the mesothelin HLE BiTE molecule for mesothelin may drive uptake in the tumor, but the uptake seems influenced by the availability in the blood after rapid clearance.

Ex vivo biodistribution revealed that ^{89}Zr-mesothelin HLE BiTE uptake was increased in multiple organs such as the liver, kidney, lung, adipose tissue, and gastrointestinal tract, compared with the control HLE BiTE. A slightly increased uptake in the liver and kidney is also found for radiolabeled antimesothelin antibodies, compared with other antibodies, in humans (37,38). Higher uptake observed in the lung, adipose tissue, and heart is consistent with RNA expression profiles of mesothelin (39). The gastrointestinal tract uptake of ^{89}Zr-mesothelin HLE BiTE is CD3-mediated with uptake in the gut-associated lymph nodes. Specific immune cell–mediated uptake in the gut has been previously observed for a murine CD8-positive T-cell tracer and a radiolabeled BiTE molecule targeting CD3-positive T cells (13,40).

Unexpectedly, the livers of mice receiving ^{89}Zr-mesothelin HLE BiTE showed an increase in necrotic areas, which was tracer dose-dependent, whereas the liver does not express mesothelin (19,39). The buffer components were similar, and we ruled out endotoxin toxicity as a cause but have yet to find an explanation for this observation. Further investigation was beyond the scope of this study.

In the clinic, BiTE molecules are administered continuously and intravenously, given their short half-life. In a PET-imaging study with ^{89}Zr-AMG 211 in patients with gastrointestinal adenocarcinomas, rapid renal clearance and relatively low tumor uptake were observed (9). With the extended half-life of HLE BiTE molecules, less frequent administrations and higher tumor uptake are projected. Multiple HLE BiTE molecules are currently being evaluated, and most have an affinity balance between CD3 and the tumor-associated antigen similar to that of the mesothelin HLE BiTE evaluated here (AMG 160, prostate-specific membrane antigen K_d = 14.8 nM and CD3 K_d = 22.4 nM; AMG 757, DLL3 K_d = 0.64 nM and CD3 K_d = 14.9 nM) (41,42).

Increasing the blood half-life of tumor-targeting antibody constructs raises the tumor uptake in mice (17). The effect of increasing tumor affinity on tumor uptake is less straightforward (16). A theoretic peak in maximum uptake seems to exist, in which a lower affinity will prevent accumulation, and increasing the affinity will hamper tumor penetration and accumulation (16,43). Therefore, we hypothesize that the extended half-life is mainly responsible

functions as the primary filter for the blood, has leaky discontinuous capillaries that permit fast accumulation (34,35). A dose of 10 μg resulted in immediate high spleen uptake, low blood levels, and moderate tumor uptake. This rapid uptake seemed to limit the available HLE BiTE molecules in the circulation. A small increase in the protein dose from 10 to 50 μg resulted in reduced spleen uptake, higher blood levels, and higher tumor uptake. Increasing the dose to 200 μg further reduced spleen uptake, but it did not further increase tumor uptake, possibly because of binding saturation. Dose-dependent uptake was not observed in the thymus, and uptake in the thymus was slower than in the spleen. In contrast to the spleen, the thymus has continuous capillaries limiting blood extravasation from the vasculature (36). Both thymus and spleen have an extensive availability of CD3-positive T cells, but dose-dependent uptake is observed just in the spleen. The 9-fold higher

for the increase in tumor uptake of the mesothelin HLE BiTE compared with canonic BiTE molecules.

CONCLUSION

It is complex to predict the contribution of each targeting arm of a bispecific antibody construct to its biodistribution. Our results indicate that the circulatory half-life of the construct plays an important role in this biodistribution. In this study, molecular imaging demonstrated that the mesothelin HLE BiTE biodistribution is driven by both targeting arms and has improved pharmacokinetic parameters over BiTE molecules. These findings support the future clinical development of HLE BiTE molecules and the use of molecular imaging in this process to understand biodistribution and tumor targeting.

DISCLOSURE

ACKNOWLEDGMENTS

KEY POINTS

QUESTION: What is the whole-body biodistribution of HLE BiTE in tumor-bearing syngeneic mice, and does it target tumors?

PERTINENT FINDINGS: This biodistribution study with a [89]Zr-labeled mesothelin-targeted HLE BiTE molecule and a [89]Zr-control HLE BiTE molecule revealed specific tumor uptake, with both targeting arms of the mesothelin HLE BiTE molecule contributing to its biodistribution. The mesothelin HLE BiTE molecule accumulated at mesothelin and CD3-expressing tissues, such as the tumor and the spleen.

IMPLICATIONS FOR PATIENT CARE: Multiple HLE BiTE molecules are currently in clinical trials. This study in mice showed that they have a favorable biodistribution profile and supports the potential for clinical translation of HLE BiTE molecules.

REFERENCES

1. Carter PJ, Lazar GA. Next generation antibody drugs: pursuit of the 'high-hanging fruit.' *Nat Rev Drug Discov.* 2018;17:197–223.

2. Suurs FV, Lub-de-Hooge MN, de Vries EGE, et al. A review of bispecific antibodies and antibody constructs in oncology and clinical challenges. *Pharmacol Ther.* 2019; 201:103–119.

3. Labrijn AF, Janmaat ML, Reichert JM, et al. Bispecific antibodies: a mechanistic review of the pipeline. *Nat Rev Drug Discov.* 2019;18:585–608.

4. Mack M, Riethmuller G, Kufer P. A small bispecific antibody construct expressed as a functional single-chain molecule with high tumor cell cytotoxicity. *Proc Natl Acad Sci USA.* 1995;92:7021–7025.

5. Klinger M, Benjamin J, Kischel R, et al. Harnessing T cells to fight cancer with BiTE(®) antibody constructs: past developments and future directions. *Immunol Rev.* 2016;270:193–208.

6. Topp MS, Duell J, Zugmaier G, et al. Anti-B-cell maturation antigen BiTE molecule AMG 420 induces responses in multiple myeloma. *J Clin Oncol.* 2020;38:775–783.

7. Hummel HD, Kufer P, Grüllich C, et al. Phase 1 study of pasotuxizumab (BAY 2010112), a PSMA-targeting bispecific T-cell engager (BiTE) immunotherapy for metastatic castration-resistant prostate cancer (mCRPC). *J Clin Oncol* [abstract]. 2019;37(suppl):5034.

8. Zhu M, Wu B, Brandl C, et al. Blinatumomab, a bispecific T-cell engager (BiTE®) for CD-19 targeted cancer immunotherapy: clinical pharmacology and its implications. *Clin Pharmacokinet.* 2016;55:1271–1288.

9. Moek KL, Waaijer SJH, Kok IC, et al. [89]Zr-labeled bispecific T-cell engager AMG 211 PET shows AMG 211 accumulation in CD3-rich tissues and clear, heterogeneous tumor uptake. *Clin Cancer Res.* 2019;25:3517–3527.

10. Arvedson TL, Balazs M, Bogner P, et al. Generation of half-life extended anti-CD33 BiTE® antibody constructs compatible with once-weekly dosing. *Cancer Res* [abstract]. 2017;77(suppl):55.

11. Lorenczewski G, Friedrich M, Kischel R, et al. Generation of a half-life extended anti-CD19 BiTE antibody construct compatible with once-weekly dosing for treatment of CD19-positive malignancies. *Blood* [abstract]. 2017;130(suppl):2815.

12. Leong SR, Sukumaran S, Hristopoulos M, et al. An anti-CD3/anti-CLL-1 bispecific antibody for the treatment of acute myeloid leukemia. *Blood.* 2017; 129:609–618.

13. Suurs FV, Lorenczewski G, Stienen S, et al. Biodistribution of a CD3/EpCAM bispecific T-cell engager is driven by the CD3 arm. *J Nucl Med.* 2020;61:1594–1601.

14. Mandikian D, Takahashi N, Lo AA, et al. Relative target affinities of T-cell-dependent bispecific antibodies determine biodistribution in a solid tumor mouse model. *Mol Cancer Ther.* 2018;17:776–785.

15. Einsele H, Borghaei H, Orlowski RZ, et al. The BiTE (Bispecific T-cell Engager) platform: development and future potential of a targeted immune-oncology therapy across tumor types. *Cancer.* 2020;126:3192–3201.

16. Warnders FJ, Lub-de Hooge MN, de Vries EGE, et al. Influence of protein properties and protein modification on biodistribution and tumor uptake of anticancer antibodies, antibody derivatives, and non-Ig scaffolds. *Med Res Rev.* 2018;38: 1837–1873.

17. Stork R, Campigna E, Robert B, et al. Biodistribution of a bispecific single-chain diabody and its half-life extended derivatives. *J Biol Chem.* 2009;284:25612–25619.

18. Heskamp S, Raavé R, Boerman O, Rijpkema M, Goncalves V, Denat F. [89]Zr-immuno-positron emission tomography in oncology: state-of- the-art [89]Zr radiochemistry. *Bioconjug Chem.* 2017;28:2211–2223.

19. Hassan R, Thomas A, Alewine C, et al. Mesothelin immunotherapy for cancer: ready for prime time? *J Clin Oncol.* 2016;34:4171–4179.

20. Sternjak A, Lee F, Wahl J, et al. Preclinical evaluation of a BiTE® antibody construct with extended half-life that targets the tumor differentiation marker mesothelin. *Cancer Res* [abstract]. 2017;77(suppl):3630.

21. Jurcak NR, Zarecki M, Lee F, et al. Evaluation of mesothelin BiTE® antibody constructs in models of pancreatic ductal adenocarcinoma. *Cancer Res* [abstract]. 2019; 79(suppl):1561.

22. Hassan R, et al. First-in-human, multicenter, phase I dose-escalation and expansion study of anti-mesothelin antibody-drug conjugate anetumab ravtansine in advanced or metastatic solid tumors. *J Clin Oncol.* 2020;38:1824–1835.

23. Morello A, Sadelain M, Adusumilli PS. Mesothelin-targeted CARs: driving T cells to solid tumors. *Cancer Discov.* 2016;6:133–146.

24. Jacobsen FW, Stevenson R, Li C, et al. Engineering an IgG scaffold lacking effector function with optimized developability. *J Biol Chem.* 2017;292:1865–1875.

25. Verel I, Visser GWM, Boellaard R, et al. [89]Zr immuno-PET: comprehensive procedures for the production of [89]Zr-labeled monoclonal antibodies. *J Nucl Med.* 2003;44: 1271–1281.

26. Steel CD, et al. Comparison of the lateral tail vein and the retro-orbital venous sinus as routes of intravenous drug delivery in a transgenic mouse model. *Lab Anim (NY).* 2008;37:26–32.

27. Yardeni T, et al. Retro-orbital injections in mice. *Lab Anim (NY).* 2011;40:155–160.

28. Warnders FJ, Waaijer SJH, Pool M, et al. Biodistribution and PET imaging of labeled bispecific T cell-engaging antibody targeting EpCAM. *J Nucl Med.* 2016;57:812–817.

29. van der Veen EL, Giesen D, Pot-de Jong L, et al. [89]Zr-pembrolizumab biodistribution is influenced by PD-1–mediated uptake in lymphoid organs. *J Immunother Cancer.* 2020;8:e000938.

30. Bankhead P, Loughrey MB, Fernandez JA, et al. QuPath: open source software for digital pathology image analysis. *Sci Rep.* 2017;7:16878.

31. Waaijer SJH, Warnders FJ, Stienen S, et al. Molecular imaging of radiolabeled bispecific T-cell engager [89]Zr-AMG211 targeting CEA-positive tumors. *Clin Cancer Res.* 2018;24:4988–4996.

32. El Hentati FZ, Gruy F, Iobagiu C, et al. Variability of CD3 membrane expression and T cell activation capacity. *Cytometry B Clin Cytom.* 2010;78:105–114.

33. Ginaldi L, Matutes E, Farahat N, et al. Differential expression of CD3 and CD7 in T-cell malignancies: a quantitative study by flow cytometry. *Br J Haematol.* 1996; 93:921–927.

34. Bronte V, Pittet M. The spleen in local and systemic regulation of immunity. *Immunity.* 2013;39:806–818.

35. Cataldi M, Vigliotti C, Mosca T, et al. Emerging role of the spleen in the pharmacokinetics of monoclonal antibodies, nanoparticles and exosomes. *Int J Mol Sci.* 2017; 18:1249.

36. Pavelka M, Roth J. *Functional Ultrastructure: Atlas of Tissue Biology and Pathology.* Springer Vienna; 2010:198, 294–298.

37. Lamberts LE, Menke-van der Houven van Oordt CW, ter Weele EJ, et al. Immuno-PET with anti-mesothelin antibody in patients with pancreatic and ovarian cancer before anti-mesothelin antibody-drug conjugate treatment. *Clin Cancer Res.* 2016; 22:1642–1652.

38. Bensch F, Smeenk MM, van Es SC, et al. Comparative biodistribution analysis across four different [89]Zr-monoclonal antibody tracers: the first step towards an imaging warehouse. *Theranostics.* 2018;8:4295–4304.

39. Uhlén M, Fagerberg L, Hallström BM, et al. Tissue-based map of the human proteome. *Science.* 2015;347:1260419.

40. Seo JW, Tavaré R, Mahakian LM, et al. CD8+ T-cell density imaging with ^{64}Cu-labeled cys-diabody informs immunotherapy protocols. *Clin Cancer Res.* 2018;24:4976–4987.

41. Bailis J, Deegen P, Thomas O, et al. Preclinical evaluation of AMG 160, a next-generation bispecific T cell engager (BiTE) targeting the prostate-specific membrane antigen PSMA for metastatic castration-resistant prostate cancer (mCRPC). *J Clin Oncol* [abstract]. 2019;37(suppl):301.

42. Giffen MJ, Cooke K, Lobenhofer EK, et al. AMG 757, a half-life extended, DLL3-targeted bispecific T-cell engager, shows high potency and sensitivity in preclinical models of small cell lung cancer. *Clin Cancer Res.* 2021;27:1526–1537.

43. Thurber GM, Schmidt MM, Wittrup KD. Antibody tumor penetration: transport opposed by systemic and antigen-mediated clearance. *Adv Drug Deliv Rev.* 2008; 60:1421–1434.